Quantifying Spatiotemporal Variability of Patna's 2023 Monsoon Flood Using Sentinel-1 SAR Data and Moran's Index

Rasheeda Soudagar[1], Aditya Kumar Thakur[1]

[1]Department of Civil Engineering, Indian Institute of Technology Roorkee, Haridwar, India - rasheeda_s@ce.iitr.ac.in; aditya_kt@ce.iitr.ac.in

Keywords: Moran's Index, Otsu thresholding, Patna floods, sentinel-1, Synthetic Aperture Radar.

Abstract

Patna, the capital of Bihar, is among the cities most severely affected by floods in India. It is primarily due to its geographic location, being bordered by the Ganga, Sone, and Punpun rivers, which significantly increases its vulnerability to flooding. Our study aims to quantify the dynamic nature of Patna's floods using statistical parameters, including global correspondence based on Moran's Index. The flood extents required for statistical analysis were generated by applying Otsu thresholding to Sentinel-1 Synthetic Aperture Radar (SAR) data in Google Earth Engine (GEE) for the 2023 monsoon period (July to October). Spline interpolation was used to smooth the data, generating a continuous curve that fits the original discrete measurements. Spatiotemporal analysis revealed significant variability in water extent, peaking at 484.13 sq. km on 3rd September and receding to 97.88 sq. km on 20th September. The correspondence values indicate a significant shift in flooded areas throughout the monsoon period. The reason may be attributed to the combined effect of change in local rainfall patterns, poor drainage system and poor flood management in the upper reaches of Ganga. Further, validation with high-resolution PlanetScope data shows an overall accuracy of 93.10% and an F1 score of 0.8416. Overall, the findings provide valuable insights into flood management and disaster preparedness in the region.

1. Introduction

Patna, a major city in India, experiences significant annual flooding, particularly during the monsoon season. This recurring issue is exacerbated by its geographical position along major rivers like the Ganga, making it highly vulnerable to water-related disasters (Khan et al., 2022; Kouser-Asif, 2022). This led to substantial economic losses and environmental damage, including deforestation, riverbank erosion, and the deterioration of water quality (Yaseen, 2024). Several studies were carried out to map and assess the reasons and impacts of the flood in Patna (Kumar and Pradhan, 2024; Kumari et al., 2024). Otsu thresholding has been a widely used flood mapping technique using SAR data, which is preferred over optical data for flood mapping due to its cloud-penetrating and day-night acquisition capabilities (Tiwari et al., 2020; Tran et al., 2022; Wayalun et al., 2012). A study found that using RS, GIS, and bivariate models like the frequency ratio and entropy models effectively mapped flood risks in the Patna district. About 16.35% (FR model) and 9.98% (SEI model) of the area are at very high flood risk, particularly in the southeast and northwest. Validation using the ROC curve confirmed the reliability of these models, showing that 13 out of 23 blocks have over 25% of their area under very high flood risk (Sarkar et al., 2022).

A study assessed flood vulnerabilities across Bihar, India, including Patna, using data from 1953 to 2020 and a composite index based on exposure, sensitivity, and adaptive capacity. The backwaters from the Ganges exacerbate waterlogging issues from Patna to Lakhisarai. Patna's higher education levels and per capita income contribute to lower flood vulnerability, guiding targeted disaster risk reduction policies. It is only focused on the city area rather than the entire district (Kumar and Pradhan, 2024). Another study reveals that the urbanization and land use changes have intensified flooding issues in Patna. Between 2005 and 2019, built-up areas increased by 22.82% while agricultural land decreased by 15.48%, leading to a rise in runoff from 16.8% to 23.72% from 2010 to 2015 (S. Ranjan et al., 2021). Severe water pollution in flood-affected areas, with high levels of contaminants, increases the severity of floods (Ravindra et al., 2024).

Sentinel-1 proved very useful in various types of disaster detection and preparedness, including land deformation, flood, land use land cover alteration, etc. (Karanam et al., 2021; Mastro et al., 2022; A. K. Ranjan et al., 2021; Ruiz-Armenteros et al., 2016; Thakur et al., 2025, 2024; Tran et al., 2022; Twele et al., 2016; Vanama et al., 2020; Zhang et al., 2023). A study uses thresholding and unsupervised classification on high-resolution multi-temporal SAR and optical images to map inundated areas during the August 2017 floods in Uttar Pradesh, India. Zonal statistical analysis was performed, and district-wise flood mapping was created and validated with meteorological data. The results demonstrate the effectiveness of SAR in flood monitoring and management (Anusha and Bharathi, 2020). Further, SAR-based flood mapping leverages more advanced methodologies like fuzzy logic, machine learning, and data fusion, which offers increased accuracy compared to traditional techniques. Recent open SAR datasets with ground-truth references enable objective validation and reproducibility. However, challenges persist in urban and vegetated areas due to complex scattering mechanisms (Amitrano et al., 2024).

A study on automatic flood mapping algorithms for areas with emerging vegetation uses single SAR acquisitions and ancillary data. It employs probability binning for statistical backscatter analysis. It also integrates land use, morphology, and context through fuzzy logic. This methodology was applied to the 2011 Condamine-Balonne floods and achieved over 80% accuracy using optical validation (Grimaldi et al., 2020). Another study using the GEE4FLOOD framework leverages Google Earth Engine, Sentinel-1 SAR imagery, and Otsu's thresholding for rapid flood mapping, tested on Kerala's 2018 flood event. It incorporates remote sensing

datasets for water mask creation and validation. The method achieved 82% overall accuracy and generated flood maps within 2–4 minutes (Vanama et al., 2020). A study evaluates the effectiveness of Sentinel-1 (SAR) and Sentinel-2 (optical) in systematic flood assessment across Europe, focusing on flood events with durations of hours to days. Using 10 years of river discharge data from ~2000 sites, it estimates the potential observation coverage of inundation events. Results show that Sentinel-1 can potentially observe 58% of flood events, while Sentinel-2 is limited to 28% due to cloud coverage (Tarpanelli et al., 2022).

The role of machine learning techniques in flood risk and impact assessments emphasises its potential to improve accuracy, reduce computation time, and lower costs. Applications include remote sensing for exposure estimation and social media analysis for flood response. Challenges like data needs, applicability, bias, and ethics are also addressed (Wagenaar et al., 2020). Flood inundation maps provide valuable information towards flood risk preparedness, management, communication, response, and mitigation during disaster (Soudagar et al., 2025). An approach was made to develop the flood risk map using satellite imagery. Sentinel-1 SAR data and the Otsu method were utilized to map flood inundation areas. Google Earth Engine (GEE) implemented the Otsu algorithm and processed Sentinel-1 SAR data. The results were assessed by calculating a confusion matrix, comparing the submerged water areas of flooded (Aug 2018), non-flooded (Jan 2018) and previous year's flooded seasons (Aug 2016, Aug 2017), and analyzing historical rainfall patterns to understand the flood event. The overall accuracy for the Sentinel-1 SAR flood inundation maps of 9th and 21st August 2018 was 94.3% and 94.1%, respectively. The submerged area (region under water) classified significant flooding as compared to the non-flooded (January 2018) and previous year's same season (August 2015–2017) classified outputs. Summing up, observations from Sentinel-1 SAR data using the Otsu algorithm in GEE can act as a powerful tool for mapping flood inundation areas at the time of the disaster, enhancing existing efforts towards saving lives and livelihoods of communities and safeguarding infrastructure and businesses (Tiwari et al., 2020; Tran et al., 2022; Wayalun et al., 2012).

Previous research often overlooked the detailed spatial distribution of floods over the monsoon period. The association between the extent of water among different dates is still unexplored. The research addresses gaps by quantifying the dynamic nature of Patna's floods using statistical parameters, particularly Moran's Index. It applies Otsu thresholding on advanced Sentinel-1 SAR processed data for precise flood mapping over time. Additionally, it accesses spatial and temporal variability of floods to access and quantifies the changing behaviour of floods. Validation was done using Cloud-free PlanetScope optical data, and parameters such as F1 score and overall accuracy were calculated to show the reliability of the result. Overall, this paper provides a profound insight into flood behaviour and can provide a robust framework for future flood risk management in the region.

2. Study Area

Patna is the capital city of Bihar and the district's administrative centre. It is one of the oldest continuously inhabited cities in the world (Alakshendra, 2019; Boyk, 2015). The city is located in the south Ganga plain and is frequently affected by monsoonal floods due to intense rainfall, River bank line changes, rapid urbanization and improper drainage system. The city is situated at an altitude of 67 meters above mean sea level, stretching between latitudes 25.22° N to 25.75° N and longitudes 84.72° E to 84.73° E. It has an area of 3,202 sq. km. with major LULC classes constituting- agriculture land, builtup area, waterbody and rangeland (Figure 1). The district features predominantly flat alluvial plain terrain, with naturally formed levees found south of the Ganga River. The Diara Plain extends across this area, making it highly vulnerable to flash floods. On the eastern side of the district, the Tal physiography is present. Flooding severely impacts the district, with some areas submerged under floodwaters reaching heights of 4 to 5 meters (Rashiq and Prakash, 2023; Ravindra et al., 2024; Sarkar et al., 2022).

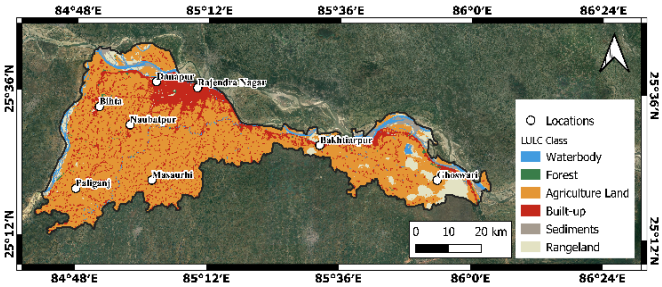

Figure1. Study area map of Patna district showing different LULC classes.

3. Methodology

3.1 Dataset

Sentinel-1 ascending pass GRD (Ground Range Detected) data with VV polarization was utilized to analyze monsoon season dynamics from August to October. Data was downloaded and processed using GEE (Google Earth Engine). The data is collected for the monsoon season, i.e. August to October, at 12-day intervals. Ten images were used during this study. Cloud-free PlanetScope optical data, with a 3-meter spatial resolution from 18/09/2023, was utilized for validation.

3.2 Processing

The methodology The overview of the methodology followed is shown in Figure 2. The Sentinel-1 GRD images of the ascending pass were pre-processed and thresholded in the GEE platform. The application of orbit files, thermal noise removal, calibration, speckle filtering, terrain correction, and decibel scale conversion were some of the preprocessing steps that were applied (Soudagar et al., 2024). The VV polarized images were used in this study to derive flood extents. The pre-processed images were cropped to match the study area extent and were classified into water and non-water classes by using Otsu thresholding (Otsu, 1979). Otsu thresholding is an automated thresholding approach where the optimal threshold is found by maximizing the between-class variance of water and non-water classes (Equation 1).

$$\sigma_{Bw}^2 = \omega_w \omega_{nw} (\mu_{w-} \mu_{nw})^2 \quad (1)$$

Where σ_{Bw}^2 is the between-class variance, ω_w and ω_{nw} are the probability of occurrence for water and non-water class, and μ_w and μ_{nw} are the class means of water and non-water classes,

respectively. Binary classified maps were generated for all the images. Water and non-water classes were represented 1 and 0, respectively. The SAR-derived flood extent of 18/09/2023 was validated against a flood reference layer generated from PlanetScope optical image acquired on the same day. Further, the extent of the area of water was calculated and used in spatial analysis. Global Moran's I formula (Equation 2) was used to calculate the extent of association between each pair.

$$G = \frac{n\sum_i\sum_j w_{ij}(x_i-\bar{x})(x_j-\bar{x})}{\sum_i(x_i-\bar{x})^2\sum_i\sum_j w_{ij}} \quad (2)$$

where n is the number of grid cells, $\sum_i\sum_j w_{ij}$ is the sum of weights, w_{ij} is the weight assigned, x_i is the water extent (1 if water is present, 0 if absent) in the cell i and x_j are the values of the spatial variables, and $\bar{x}$ is the mean value of the variable. In this context, the spatial association function of Arc-GIS Pro was applied between the Input zone, i.e., the water extent map of previous dates, and the Overlay zone, i.e., the water extent map of later dates.

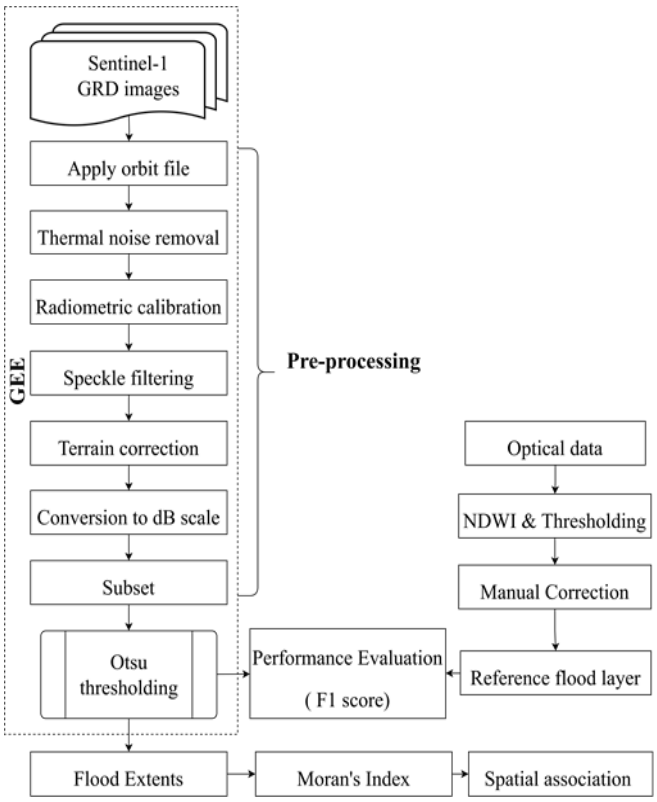

Figure 2. Methodological flowchart showing various steps involved in the study.

4. Results and Discussions

4.1. Flood extent generation

The flood extent maps were generated in GEE using the Otsu thresholding technique. The spatial and temporal variation of flood extent is shown in Figure. 3. The Otsu thresholding technique works by maximising the between-class variance, which is the difference between the mean values of the water and non-water classes, providing an optimal threshold for classification. The optimal threshold values for each image used for distinguishing flooded areas for different captures are represented in Table 1.

Table 1. Optimal threshold values for each image

Date	Threshold Value (dB)	Date	Threshold Value (dB)
08th July	-12.856	06th Sept	-10.903
20th July	-12.877	18th Sept	-16.879
01st Aug	-12.883	30th Sept	-12.831
13th Aug	-14.874	12th Oct	-12.847
25th Aug	-12.887	24th Oct	-12.864

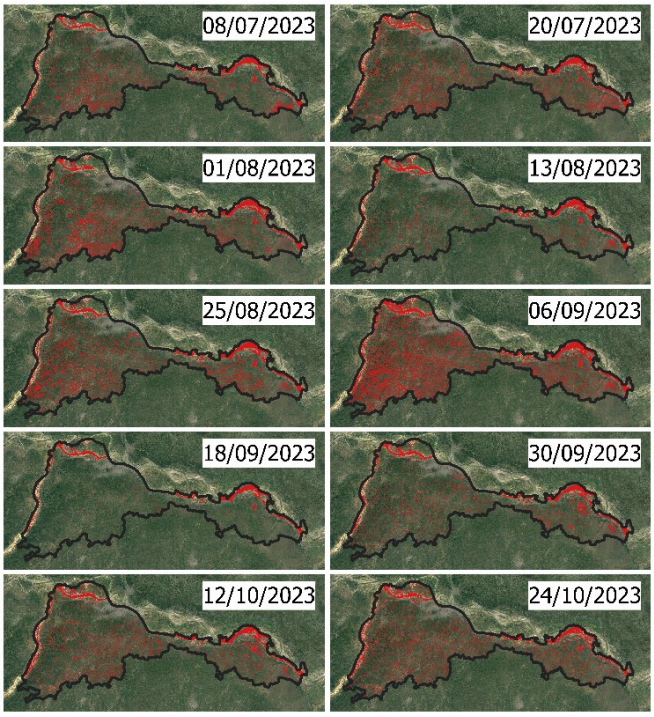

Figure 3. Spatio-temporal distribution of flood for Patna (Red indicates flood).

The flood extents were validated against the flood reference layer generated from the cloud-free PlanetScope optical image acquired on 18/09/2023. The NDWI image was formed using Green and NIR bands. Further, the NDWI image was segmented into water and non-water class using thresholding and manual digitization. The true colour composite of PlanetScope image is shown in Fig. 4 (a) and the corresponding flood reference layer is shown in Fig. 4 (b). We carried out pixel to pixel validation of generated flood extent of 18/09/2023 with flood reference layer. Upon validation an overall accuracy of 93.10% and F1 score of 0.8416 were obtained. Precision and recall are 0.9853 and 0.7345, respectively.

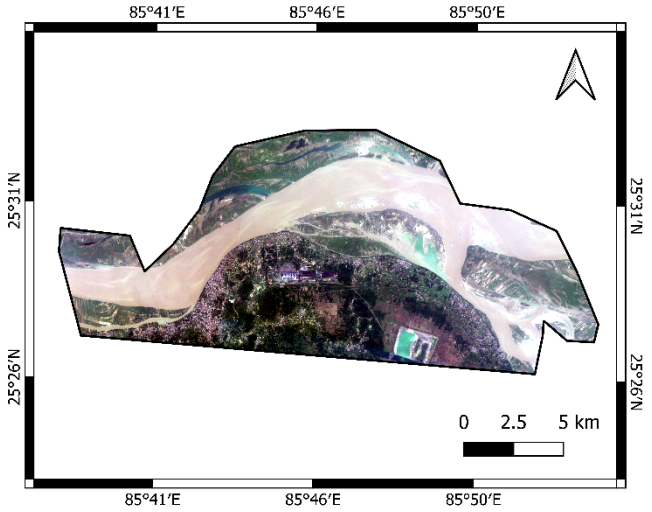

(a)

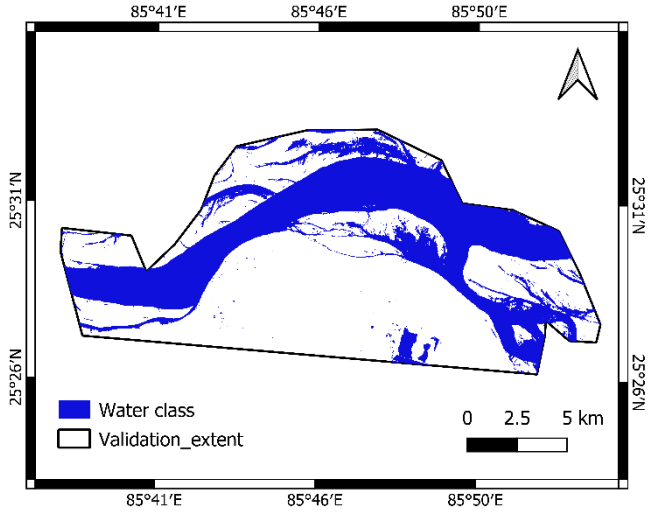

(b)

Figure 4. Validation of data from planet imagery. (a) True color composite of PlanetScope scene. (b) Labels generated from PlanetScope imagery for validation.

4.2. Value-Based Analysis

Table 2: Spatial statistics of measured water extent for Patna for different dates in 2023.

Date	Water extent (sq.km.)	Date	Water extent (sq.km.)
08th July	215.32	06th September	470.27
20th July	306.89	18th September	116.31
01st August	299.44	30th September	213.23
13th August	209.10	12th October	239.49
25th August	320.37	24th October	268.83

Table 2 presents the spatial statistics of water extent in the Patna district for various dates during the study period. Spline interpolation was used to smooth the data, generating a continuous curve that fits the original discrete measurements (Figure 5). This smooth curve enables the calculation of statistical values, with the mean, maximum, and minimum water extents derived from it. The mean water extent over the period was 267.98 sq. km. The maximum water extent of 484.13 sq. km. was observed on 3rd September 2023, suggesting a major flood event or heavy rainfall within the city likely occurred during early September. It is possibly due to heavy monsoon rains and Ganga River inundation. Conversely, the minimum water extent of 97.88 sq. km. was recorded on 20th September 2023, indicating a period of floodwater recession likely resulting from reduced rainfall or improved drainage. The dates corresponding to these extremes are identified by mapping their indices back to the original time axis. The variation in water extent across the monsoon period reflects the dynamic nature of flooding in the region.

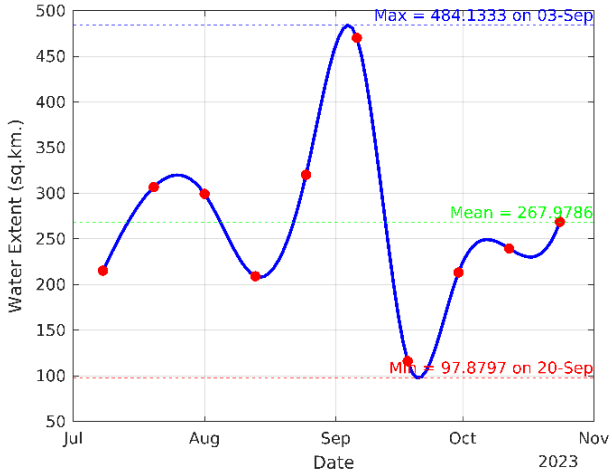

Figure 5. Variation of the flooded area within the study period.

4.3. Area-Based Analysis

Table 2: Global correspondence between the water extent of different dates of 2023.

2023	08/07	01/08	25/08	18/09
01/08	0.1029			
25/08	0.0744	0.1036		
18/09	0.2167	0.1906	0.2355	
12/10	0.0988	0.0939	0.0978	0.2754

The global correspondence values from Table 2 show how similar the water extents were between different dates. For continuous change detection, interpolation was applied to the correspondence matrix by normalizing the values to a [0, 1] range. A denser grid of query points was created using a mesh grid, and interp2 was used to estimate values at these points through spline interpolation. This results in a smooth representation of the data. Finally, the interpolated values were clamped to ensure they remained within the [0, 1] range, creating a continuous and visually interpretable map of correspondence between dates (Figure 6).

Higher values, such as 0.2754 between 18th September and 12th October, indicate that the water extent remained relatively consistent during these periods, likely due to sustained flooding or slow recession of floodwaters. Lower correspondence values, such as 0.0744 between 08th July and 25th August, suggest significant changes in water extent, possibly due to fluctuating rainfall and varying flood intensities. The variations in water extent and global

correspondence can be attributed to the combined effects of Ganga River inundation and localized waterlogging. The rise in water extent in early September coincides with the peak of the monsoon season, when the Ganga River often overflows, causing widespread flooding.

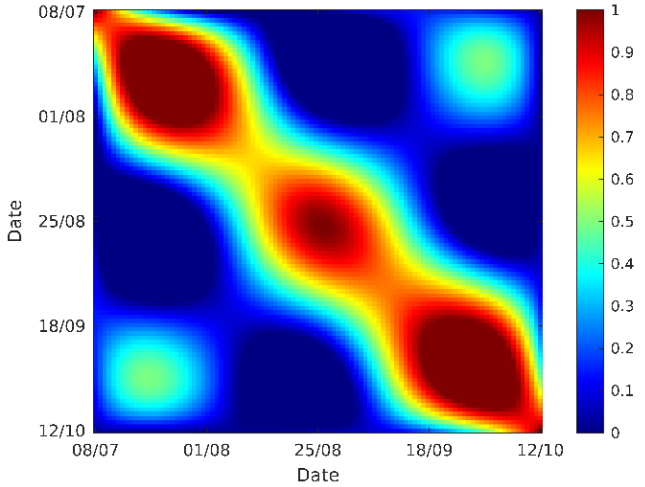

Figure 6. Global correspondence plot for flooded areas of different dates within the study period.

5. Conclusion

In 2023, the Patna district experienced significant spatiotemporal variability in water extent due to flooding and waterlogging, as illustrated by the measured areas of water coverage and their global correspondence across different dates. The water extent fluctuated considerably, peaking at 484.13 sq. km. on 03rd September, which likely marks the height of the monsoon season and river inundation. This was followed by a sharp decrease, indicating rapid water recession, although some areas remained persistently waterlogged, as evidenced by the still considerable water extent in October. The global correspondence values reveal that the water extent varied widely between certain dates, particularly earlier in the season, with lower correspondence values such as 0.0744 between 08th July and 25th August. In contrast, later dates showed higher correspondence, such as 0.2754 between 18th September and 12th October, indicating more stable or prolonged flooding conditions. These findings underscore the complex dynamics of flooding in Patna, driven by varying rainfall patterns, river behaviour, and the district's drainage capacity. This study can be further expanded by incorporating hydrological and meteorological factors such as rainfall intensity, river discharge, and soil moisture to provide a more comprehensive understanding of flood dynamics.

Acknowledgement

The authors express their gratitude to the Indian Institute of Technology Roorkee for providing the environment and facilities necessary for conducting this research work. We also extend our thanks to all those who contributed directly or indirectly to the successful completion of this work.

References

Alakshendra, A., 2019. City Profile: Patna, India. Environ. Urban. ASIA 10, 374–392.

Amitrano, D., Di Martino, G., Di Simone, A., Imperatore, P., 2024. Flood detection with SAR: A review of techniques and datasets. Remote Sens. 16, 656.

Anusha, N., Bharathi, B., 2020. Flood detection and flood mapping using multi-temporal synthetic aperture radar and optical data. Egypt. J. Remote Sens. Space Sci. 23, 207–219.

Boyk, D.S., 2015. Provincial Urbanity: Intellectuals and Public Life in Patna, 1880-1930.

Grimaldi, S., Xu, J., Li, Y., Pauwels, V.R.N., Walker, J.P., 2020. Flood mapping under vegetation using single SAR acquisitions. Remote Sens. Environ. 237, 111582.

Karanam, V., Motagh, M., Garg, S., Jain, K., 2021. Multi-sensor remote sensing analysis of coal fire induced land subsidence in Jharia Coalfields, Jharkhand, India. Int. J. Appl. Earth Obs. Geoinformation 102, 102439. https://doi.org/10.1016/j.jag.2021.102439

Khan, A., Govil, H., Khan, H.H., Thakur, P.K., Yunus, A.P., Pani, P., 2022. Channel responses to flooding of Ganga River, Bihar India, 2019 using SAR and optical remote sensing. Adv. Space Res. 69, 1930–1947.

Kouser-Asif, S., 2022. Extreme flood events in India and attribution to climate change: an analysis of news media coverage from 2013–2019 during Bihar floods. Nat. Hazards Rev. 23, 5021018.

Kumar, G.D., Pradhan, K.C., 2024. Assessing the district-level flood vulnerability in Bihar, eastern India: an integrated socioeconomic and environmental approach. Environ. Monit. Assess. 196, 799.

Kumari, N., Dhiman, R., Krishnankutty, M., Kalbar, P., 2024. Localising vulnerability assessment to urban floods: A comparative analysis of top-down and bottom-up geospatial approaches in Patna City, India. Int. J. Disaster Risk Reduct. 100, 104230.

Mastro, P., Masiello, G., Serio, C., Pepe, A., 2022. Change Detection Techniques with Synthetic Aperture Radar Images: Experiments with Random Forests and Sentinel-1 Observations. Remote Sens. 14. https://doi.org/10.3390/rs14143323

Otsu, N., 1979. A Threshold Selection Method from Gray-Level Histograms. IEEE Trans. Syst. Man Cybern. 9, 62–66. https://doi.org/10.1109/TSMC.1979.4310076

Ranjan, A.K., Sahoo, D., Gorai, A.K., 2021. Quantitative assessment of landscape transformation due to coal mining activity using earth observation satellite data in Jharsuguda coal mining region, Odisha, India. Environ. Dev. Sustain. 23, 4484–4499. https://doi.org/10.1007/s10668-020-00784-0

Ranjan, S., Danish, I.M., Singh, V., 2021. Impact of Land Use Changes on Urban Flooding in Patna City, in: International Conference on Hydraulics, Water Resources and Coastal Engineering. Springer, pp. 253–260.

Rashiq, A., Prakash, O., 2023. Urban floods: A case study of Patna floods 2019–Natural or anthropogenic?, in: Impacts of Urbanization on Hydrological Systems in India. Springer, pp. 57–78.

Ravindra, K., Vig, N., Chhoden, K., Singh, R., Kishor, K., Maurya, N.S., Narayan, S., Mor, S., 2024. Impact of massive flood on drinking water quality and community health

risk assessment in Patna, Bihar, India. Sustain. Water Resour. Manag. 10, 104.

Ruiz-Armenteros, A.M., Bakon, M., Lazecky, M., Delgado, J.M., Sousa, J.J., Perissin, D., Caro-Cuenca, M., 2016. Multi-Temporal InSAR Processing Comparison in Presence of High Topography. Procedia Comput. Sci. 100, 1181–1190. https://doi.org/10.1016/j.procs.2016.09.278

Sarkar, D., Saha, S., Mondal, P., 2022. GIS-based frequency ratio and Shannon’s entropy techniques for flood vulnerability assessment in Patna district, Central Bihar, India. Int. J. Environ. Sci. Technol. 19, 8911–8932.

Soudagar, R., Chowdhury, A., Bhardwaj, A., 2025. Enhanced large-scale flood mapping using data-efficient unsupervised framework based on morphological active contour model and single synthetic aperture radar image. J. Environ. Manage. 380, 124836. https://doi.org/10.1016/j.jenvman.2025.124836

Soudagar, R., Chowdhury, A., Bhardwaj, A., 2024. Application of Morphological Active Contour Model for Flood Extent Mapping Using Unitemporal SAR Image: 2023 North Indian Floods, in: IGARSS 2024 - 2024 IEEE International Geoscience and Remote Sensing Symposium. Presented at the IGARSS 2024 - 2024 IEEE International Geoscience and Remote Sensing Symposium, pp. 1200–1204. https://doi.org/10.1109/IGARSS53475.2024.10642552

Tarpanelli, A., Mondini, A.C., Camici, S., 2022. Effectiveness of Sentinel-1 and Sentinel-2 for flood detection assessment in Europe. Nat. Hazards Earth Syst. Sci. 22, 2473–2489.

Thakur, A.K., Attri, L., Garg, R.D., Jain, K., Kumar, D., Chowdhury, A., 2024. Temporal and Spatial Dynamics of Subsidence in Eastern Jharia, India, in: ISPRS Annals of the Photogrammetry, Remote Sensing and Spatial Information Sciences. Copernicus Publications Göttingen, Germany, pp. 349–356.

Thakur, A.K., Garg, R.D., Jain, K., 2025. An Assessment of Different Line-of-Sight and Ground Velocity Distributions for a Comprehensive Understanding of Ground Deformation Patterns in East Jharia Coalfield. Remote Sens. Appl. Soc. Environ. 101446.

Tiwari, V., Kumar, V., Matin, M.A., Thapa, A., Ellenburg, W.L., Gupta, N., Thapa, S., 2020. Flood inundation mapping-Kerala 2018; Harnessing the power of SAR, automatic threshold detection method and Google Earth Engine. PLoS One 15, e0237324.

Tran, K.H., Menenti, M., Jia, L., 2022. Surface water mapping and flood monitoring in the Mekong Delta using sentinel-1 SAR time series and Otsu threshold. Remote Sens. 14, 5721.

Twele, A., Cao, W., Plank, S., Martinis, S., 2016. Sentinel-1-based flood mapping: a fully automated processing chain. Int. J. Remote Sens. 37, 2990–3004.

Vanama, V.S.K., Mandal, D., Rao, Y.S., 2020. GEE4FLOOD: rapid mapping of flood areas using temporal Sentinel-1 SAR images with Google Earth Engine cloud platform. J. Appl. Remote Sens. 14, 34505.

Wagenaar, D., Curran, A., Balbi, M., Bhardwaj, A., Soden, R., Hartato, E., Mestav Sarica, G., Ruangpan, L., Molinario, G., Lallemant, D., 2020. Invited perspectives: How machine learning will change flood risk and impact assessment. Nat. Hazards Earth Syst. Sci. 20, 1149–1161.

Wayalun, P., Chomphuwiset, P., Laopracha, N., Wanchanthuek, P., 2012. Images Enhancement of G-band Chromosome Using histogram equalization, OTSU thresholding, morphological dilation and flood fill techniques, in: 2012 8th International Conference on Computing and Networking Technology (INC, ICCIS and ICMIC). IEEE, pp. 163–168.

Yaseen, Z.M., 2024. Flood hazards and susceptibility detection for Ganga river, Bihar state, India: Employment of remote sensing and statistical approaches. Results Eng. 21, 101665. https://doi.org/10.1016/j.rineng.2023.101665

Zhang, J., Ke, C., Shen, X., Lin, J., Wang, R., 2023. Monitoring Land Subsidence along the Subways in Shanghai on the Basis of Time-Series InSAR. Remote Sens. 15, 1–20. https://doi.org/10.3390/rs15040908